Investigating the relationships between chemical element concentrations and discharge to improve our understanding of their transport patterns in rural catchments under subtropical climate conditions

Cláudia A.P. de Barros, Tales Tiecher, Rafael Ramon, Danilo R. dos Santos, Marcos A Bender, O. Evrard, Sophie Ayrault, Jean P.G. Minella

Investigating the relationships between chemical element concentrations and discharge to improve our understanding of their transport patterns in rural catchments under subtropical climate conditions

Cláudia A P de Barros[a], Tales Tiecher[a], Rafael Ramon[a], Danilo R dos Santos[b], Marcos A Bender[c], Olivier Evrard[d], Sophie Ayrault[d] & Jean P G Minella[b]

[a] Soil Department, Federal University of Rio Grande do Sul (UFRGS), Interdisciplinary Research Group on Environmental Biogeochemistry (IRGEB), Bento Gonçalves Ave. 7712, 91540-000, Porto Alegre, RS, Brazil, claudia.barros@ufrgs.br, tales.tiecher@ufrgs.br, rafaramon11@gmail.com

[b] Soil Department, Federal University of Santa Maria (UFSM), Roraima Ave. 1000, 97105-900 Santa Maria, RS, Brazil, danilonesaf@gmail.com, jminella@gmail.com

[c] Agronomist Engineer, EMATER-ASCAR/RS, Botafogo street 1051, 90150-052, Porto Alegre, RS, Brazil, marcosantoniobender@yahoo.com.br

[d] Laboratoire des Sciences et de l'Environnement (LSCE-IPSL), UMR 8212 (CEA/CNRS/UVSQ), Université Paris-Saclay, CEA Saclay, Orme des Merisiers, 91 191 Gif-sur-Yvette Cedex, France, olivier.evrard@lsce.ipsl.fr, sophie.ayrault@lsce.ipsl.fr

Corresponding Author: Cláudia A P de Barros, e-mail: claudia.barros@ufrgs.br

Abstract - Solute and particulate elemental concentrations (C) exhibit different responses to changes in discharge (Q), and those relationships are not well understood in subtropical agricultural environments. The objective is to describe the transport processes of different chemical elements during a set of contrasted rainfall events (2011-2015) that occurred in a small rural catchment under subtropical climate. The study was carried out in the Lajeado Ferreira Creek catchment (1.23 km²), southern Brazil. To this end, the concentrations in dissolved organic carbon (DOC), Cl^-, NO_3^-, SO_4^- , ten chemical elements (in either dissolved or particulate forms) and suspended sediment concentrations

(SSC) were determined. Metric indices were then calculated to characterize their transport patterns: (i) the best fit slope between log-C and log-Q (β), (ii) the coefficient of variation of C and Q, (iii) shape of the hysteresis loop and hysteresis index, and (iv) the flushing index. All particulate elements along with the dissolved inorganic phosphorus (PO_4^{-3}) were shown to be controlled by the sediment dynamics. Geogenic elements (Fe^{2+}, Zn^{2+}, Cu^{2+}, Mn^{2+}, Si^{4+}) showed a dilution effect with increasing Q values, likely because they were mainly transported with subsurface and base flow. Dissolved elements that are mainly supplied with fertilizers (Na^+ and Cl^-) as well as DOC showed a dilution effect, although they were mainly transported by surface runoff. Finally, a chemostatic behavior was found for those chemical elements (Mg^{2+}, K^+, Ca^{2+}, NO_3^- and SO_4^{2-}) that are supplied by more than one flow pathways. The results demonstrate that under subtropical climate conditions, the transport of essential nutrients including PO_4^{-3} and metals (in particulate form), are mainly transported with surface runoff. Accordingly, runoff control on cultivated hillslopes should be improved to reduce the potential contaminant supply to the river and to reduce the potentially deleterious impacts that they may cause in downstream regions.

Keywords: rainfall events; export regimes; solutes; metric indexes; water quality

1. INTRODUCTION

The intensification of agricultural activities and the limited adoption of soil and water conservation practices have increased the formation of surface runoff and accelerated soil erosion (Deuschle et al., 2019; Londero et al., 2018),

sediment, nutrient and metal transport in river systems draining agricultural land around the world (Basu et al., 2010; Minella et al., 2018; Williams et al., 2018). Chemical elements supplied in excess to the streams may originate from anthropogenic activities, including agriculture through the supply of fertilizers and agrochemicals (Thomas et al., 2016), or from natural sources, as the result of rock weathering and leaching (Verheyen et al., 2015). The relationships observed between the chemical element concentrations (C) and water discharge (Q) result from the combined integration of biogeochemical processes, the contribution of the sources, flow pathways, and factors such as lithology, soil type and climate (Godsey et al., 2009; Knapp et al., 2020; Rumsey et al., 2017; Verheyen et al., 2015; Von Freyberg et al., 2017). Quantifying these relationships may contribute to improve our understanding of the transport of solutes and particulate chemical substances from upper catchment parts to the outlet.

The source of each element can be identified by reconstructing the hysteresis phenomenon based on the C – Q relationship (Lloyd et al., 2016; Wymore et al., 2019). Hysteresis analyses have been widely used and progressively improved during the last several decades and they provide a powerful technique for identifying the sources of both particle-bound (Duvert et al., 2010; Lawler et al., 2006; Wymore et al., 2019) and dissolved substances (Lloyd et al., 2016; Williams et al., 2018). Hysteresis occurs when concentrations of an element, observed in either dissolved or particulate form, during the rising stage of the hydrograph differ from those concentrations recorded at the same discharge rate during the falling stage. The hysteresis can be observed by the formation of a loop when plotting C *vs* Q.

There are three main potential interpretations of a given hysteresis loop (Lloyd et al., 2016). Clockwise hysteresis suggests the rapid mobilization of the chemical element of interest and the proximity of its source to the catchment outlet. This situation occurs when higher concentrations are observed during the event rising stage. However, when the loop is counterclockwise (i.e. when the concentration of an element is lower in the rising limb while increasing in the falling limb), the source of the chemical elements is expected to be located far from the catchment outlet. Furthermore, the eight-type hysteresis loop can be a sequence of clockwise and counterclockwise patterns. In addition, Lawler et al. (2006) proposed the hysteresis index (HI) which varies according to the magnitude of the rainfall event itself and, consequently, to the hydrological dynamics of the catchment.

Recently, metric indices have been used to evaluate these C - Q relationships, including (i) the best fit slope (β) for the log (C) - log (Q) linear regression (Godsey et al., 2009); (ii) the ratio of the concentration and water discharge coefficients of variation (CV_C/CV_Q) (Thompson et al., 2011); (iii) and a combination of both indicators (Musolff et al., 2015). The combination of both metric indices (β and CV_C/CV_Q) results in an unique structure for the interpretation of transport patterns (Musolff et al., 2015): they can be (i) chemostatic (no change in element concentration with the increase or decrease in Q), (ii) they can show a chemodynamic dilution (as Q increases, the concentration of the chemical element is reduced), (iii) or display a chemodynamic enrichment (increase in the concentration of chemical elements with increasing Q). Besides these types of behavior, the flushing index (FI), which ranges between -1 and 1, quantifies the changes in concentrations

105 during a rainfall event (Rose et al., 2018; Vaughan et al., 2019). Negative FI
106 values indicate that concentrations decrease during the hydrograph's rising
107 limb. In contrast, positive FI values indicate increased concentrations during the
108 hydrograph's rising limb. The interpretation of these indices may reveal the
109 different transport patterns of the chemical elements that may be measured
110 during the monitoring of rainfall events.

111 From this new approach, Rose et al. (2018) distinguished the following
112 transport patterns: dilution for geogenic/exogenous elements (Ca^{2+}, Mg^{2+}, Si^{4+},
113 Cl^-, NO_3^-); constant pattern for biologically associated solutes (carbon and
114 dissolved nitrogen, NH_4^+, K^+, PO_4^{3-}); and enrichment for particulate substances
115 (suspended solids and total) in a dataset covering 11 years collected in
116 Pennsylvania (USA). Through the CV_C/CV_Q ratio and based on a set of seven-
117 year rainfall events monitored in southern Brazil, Piazza et al. (2018) showed
118 that the export dynamics of solutes were similar in agricultural and in native
119 forest catchments. In South Florida, a combined analysis between the CV_C/CV_Q
120 and β showed that total nitrogen (TN) presented a chemostatic behavior while
121 total phosphorus (TP) was chemodynamic; this was due to a combination of
122 fertilizer doses, low P retention in the soil and high storms (Wan et al., 2017).

123 In subtropical and tropical climate conditions, the relationship between C
124 and Q is not well known at the event-scale. In these environments the annual
125 average rainfall volume is high as well as the kinetic energy (Ramon et al.,
126 2017), which can impact the C - Q relations during rainfall events. However,
127 there is little information on the event scale for these climates. Gwenzi et al.
128 (2017) reports the scarcity of information on the scale of hydrological (Q) and
129 biogeochemistry events for tropical climate, more precisely in Africa. In Brazil,

water quality monitoring programs generally collect samples only four times per year following a routine schedule, due to limited human and financial resources applied in this program, where the measurements do not usually occur during events. Few research efforts sought to understand the influence of climate and land use conditions on the dynamics of solute transport under these environmental conditions (Piazza et al., 2018). Agriculture is the main economic activity in the Southern region of Brazil (CONAB, 2019), resulting in a high pressure on natural resources, especially soil and water. Consequently, the environmental impact of this activity must be a constant concern, where the limited adoption of conservationist agriculture associated with the erosive potential of the rains in the region, increase the degree of soil and water degradation (Didoné et al., 2015; Merten et al., 2015). Therefore, it is important to know the hydrological and biogeochemical behavior of rural catchments in a subtropical climate like in southern Brazil, where there is no prior knowledge on the subject.

In this study, we aim to investigate the transport processes of different chemical elements during a set of contrasted rainfall events through the analysis of their C - Q relationships. For this purpose, a program to monitor the transport of chemical elements in a small rural catchment representative of those environments found on the Southern Plateau of Brazil and in neighboring regions, under subtropical climate conditions, was established in the period between 2011 and 2015.

2. MATERIALS AND METHODS

2.1 Study area

155 The experimental catchment of the Lajeado Ferreira Creek – Arvorezinha
156 (1.23 km²), is located on the border of the Brazilian southern plateau (Figure 1).
157 This is a typical headwater catchment of the Jacuí River, one of the main
158 tributaries of the Guaíba lake, which supplies drinking water to more than 4
159 million people (Cargnin et al., 2013). Its altitude ranges from 580 to 730 m
160 (Figure 1). The upper third of the catchment has an undulating plateau relief
161 with slopes up to 7%. The middle and lower thirds of the catchment have a
162 much steeper topography with slope gradients often exceeding 15%.
163 The climate is classified as Cfb (subtropical super-humid with no dry
164 season and warm summer) according to Köppen (Alvares et al., 2013). The
165 average annual rainfall is ca. 1,938 mm (15 years, 2002 - 2016) and erosivity
166 index (EI_{30}) is 9,344 MJ mm ha^{-1} yr^{-1} (Ramon, 2017). Rainfall is well distributed
167 over the year, although a wetter season with more rainfall events of high
168 intensity can be identified during the spring season with the frequent occurrence
169 of surface runoff.
170 The soil types in the catchment are Acrisols (57%), Cambisols (10%) and
171 Leptosols (33%). The spatial and temporal variability of land use and soil
172 management was determined using a combination of satellite images and field
173 surveys using a handheld Global Positioning System device. Land use and soil
174 management in 2011 included native forest (15% of the total catchment surface
175 area), reforested zones (23.2%), pasture (6.5%), cropland (soybean + tobacco)
176 under minimum tillage (26%), cropland under conventional tillage (13%), fallow
177 (13%) and other minor uses (3.3 %). By 2015, land use and soil management
178 had significantly changed, mainly through an increase in reforested areas
179 (35%), a decrease in cropland under minimum tillage (15%), while the cropland

surface proportion under conventional tillage increased to 24%, and that under fallow decreased to 2.2%. In contrast, the respective surface areas under native forest, pasture, and other land uses did not change.

2.2 Hydro-sedimentary monitoring

The Arvorezinha catchment has been monitored since 2002, with the continuous measurement of flow discharge (Q) and suspended sediment concentrations (SSC) at the outlet of the catchment in a Parshall type flume built in concrete with a 1.83 m width in its narrowest part. Water level and turbidity were recorded through a float-type water level sensor (Thalimedes, OTT HydroMet, Germany) and a turbidimeter (Model SL-2000, Solar®, Brazil), respectively. All automatic equipment recorded data every 10 minutes. SSC data were obtained by the turbidimeter properly calibrated with samples collected manually using an isokinetic sampler (US DH-48) during rainfall-runoff events as proposed by Merten et al. (2014). The 10 min interval data was used to calculate the variations of the sediment yield throughout the year. Rainfall intensity and depth have been measured by means of tipping bucket rain gauges and pluviometers, respectively, and their location is shown in Figure 1. The rainfall of the last five days (R5) before the rainfall events analyzed was computed to reflect the antecedent soil moisture conditions (SILVEIRA et al., 2000), which is classified into three classes according to rainfall volume: 1) dry when R5 < 36 mm; 2) field capacity when R5 > 36 and < 53 mm; and 3) saturated when R5 > 53 mm.

The runoff separation (the separation of surface runoff and base flow contributions) was performed for the 16 rainfall events monitored, using the graphical analysis method of Chow et al. (1988). The onset of the surface runoff

205 is determined by the rise of the hydrograph until the moment when the
206 discharge returned to values close to those observed just before the rising limb,
207 thus characterizing the end of the rainfall event.
208
209 2.3 Sampling and chemical analysis
210 During the rainfall - runoff events, 164 water samples were collected at
211 the catchment outlet using a isokinetic sampler. Duplicate samples were
212 collected, one of them to calculate the sediment concentration following the
213 evaporation method according to Shreve and Downs (2005) and the second
214 sample was used for determining the water chemical composition, which is
215 described in section 2.3.1.
216
217 2.3.1 Chemical analysis
218 In the laboratory, an aliquot of the sample was filtered at 0.22 µm to
219 characterize the dissolved fraction. The total element concentration was
220 determined in the non-filtered samples. Then, the particulate fraction was
221 obtained through calculating the difference between total and dissolved
222 concentrations.
223 In the filtered sample, the dissolved organic carbon (DOC) content was
224 determined after mixing an aliquot of the filtered sample with a 1:1
225 sulphochromic solution incubated in an oven for 4 h at 60°C, with a
226 spectrophotometer at 580 nm. Sulphate (SO_4^{2-}), chlorine (Cl^-) and nitrate (NO_3^-
227) contents were measured with a high-performance liquid chromatography
228 (HPLC) - Sykam S 135 Ion Chromatography System (U.S. EPA, 1997). Finally,
229 the concentration of dissolved Ca^{2+}, Cu^{2+}, Fe^{2+}, K^+, Mg^{2+}, Mn^{2+}, Na^+, PO_4^{3-}, Si^{4+},

and Zn^{2+} was quantified by Inductively Coupled Plasma - Optical Emission Spectrometry (ICP-OES, Perkin-Elmer) directly in the filtered water sample (U.S. EPA, 1994).

Total content in unfiltered samples of water + sediments was assessed after digestion with *aqua-regia* (U.S. EPA, 1996). In brief, a 20 mL aliquot of unfiltered sample of water + sediment was inserted into Teflon tubes together with 0.5 mL of HCl (37%) and 1 mL of HNO_3 (65%), followed by microwave assisted digestion for 9.5 min at a temperature of 182 °C. After that, Ca, Cu, Fe, K, Mg, Mn, Na, P, Si and Zn were quantified using Inductively Coupled Plasma Optical Emission Spectrometry (ICP-OES, Perkin-Elmer) (U.S. EPA, 1997). Then, particulate contents of these elements were obtained by calculating the difference between total and dissolved contents.

2.4 Data analysis

The relationship between the element concentrations and the water discharge was evaluated by means of metric indices: slope (β), CV_C/CV_Q, qualitative (loop) and hysteresis index. The analyses were performed for the 16 rainfall events monitored, evaluating the SSC, DOC, NO_3^-, SO_4^{2-}, Cl^- and the ten chemical elements analyzed (Ca^{2+}, Cu^{2+}, Fe^{2+}, K^+, Mg^{2+}, Mn^{2+}, Na^+, Zn^{2+}, PO_4^{-3}, Si^{4+}).

2.4.1 Metric indexes

To obtain the β, all Q and C data were log transformed. Accordingly, a β value was obtained for each element for the 16 rainfall events. A negative β value reflects the decrease of element concentration with the increase of Q,

255 whereas positive values indicate an increase of both C and Q. When β ~ 0, it
256 indicates a chemostatic behavior of the element. The chemostatic pattern was
257 defined when the β was considered to be significantly different from zero, at α =
258 0.05 if Student's *t* statistic | t | > 2 (Helsel and Hirsch, 2002; Rose et al., 2018).
259 The coefficient of variation of the concentration in each chemical element
260 was calculated (CV_C), as well as the coefficient of variation of water discharge
261 (CV_Q). The CV_C/CV_Q metric index indicates whether the behavior of the element
262 is chemostatic ($CV_C/CV_Q \leq 0.5$), or chemodynamic ($CV_C/CV_Q > 0.5$). According
263 to Musolff et al. (2015) both β and CV_C/CV_Q need to be evaluated in
264 combination.
265 In addition, we also examined hysteresis patterns in dissolved and
266 particulate form of the elements during individual rainfall events, as well as the
267 hysteresis index (HI), with the method of Lawler et al. (2006). The method is
268 based on measuring the width of the hysteresis loop in the central water
269 discharge (Q_{50}), when there is a 50% increment of the Q compared to the
270 beginning of the rainfall event. The Q_{50} is calculated with equation 1, based on
271 the minimum (Q_{min}) and maximum water discharge (Q_{max}) values during the
272 rainfall event.
273

$$Q_{50} = 0.5 \times (Q_{max} - Q_{min}) + Q_{min} \quad (1)$$

274
275 Thus, with the Q_{50} calculated, the chemical element concentration and
276 SCC for the exact corresponding moment was obtained by a coumpound rule of
277 three, using the closest sample collected before and after the Q_{50} time in the
278 rising and falling limbs. Therefore, HI was calculated according to equations 2
279 and 3, when the concentration in the rising limb - RL is higher than in the falling

limb - FL (clockwise hysteresis) and RL < FL (counterclockwise hysteresis), respectively.

$$HI = \left(\frac{RL}{FL}\right) - 1 \quad (2)$$

$$HI = \left(\frac{-1}{\frac{RL}{FL}}\right) + 1 \quad (3)$$

Where: RL is the element concentration in water discharge on the rising limb of the hydrograph and FL is the concentration on the falling limb.

The Flushing Index (FI) was calculated according to the method of (Vaughan et al., 2019) (Equation 4). The water discharge and the element concentration had to be normalized, according to equations 5 and 6, respectively.

$$FI = C_{Qpeak,normal} - C_{initial,normal} \quad (4)$$

Where: $C_{Qpeak,normal}$ and $C_{initial,normal}$ are the normalized elements during the peak and the beginning of each rainfall event, respectively.

$$Q_{i,normal} = \frac{Q_i - Q_{min}}{Q_{max} - Q_{min}} \quad (5)$$

$$C_{i,normal} = \frac{C_i - C_{min}}{C_{max} - C_{min}} \quad (6)$$

Where: Q_i and C_i are the water discharge and element values at time step i, respectively, Q_{max} and Q_{min} are the maximum and minimum water

298 discharge values during the rainfall event, respectively, and C_{max} and C_{min} are
299 the maximum and minimum concentrations of each element during the rainfall
300 event, respectively.
301
302 **3. RESULTS**
303 3.1 Hydro-sedimentary monitoring and element concentration
304 Table 1 shows the main characteristics of the 16 rainfall events
305 monitored between 2011 and 2015. The peak flow varied from 35 to 3,399 L s^{-1}
306 while the maximum suspended sediment concentrations fluctuated from 0.1 to
307 5.4 g L^{-1}. The magnitude of peak flows followed the magnitude of the volume
308 and duration of rainfall (Table 1). However, it is important to consider the effect
309 of the previous events on the hydro-sedimentary dynamics, because even with
310 low rainfall volume, surface runoff generation, sediment and chemical element
311 transport may occur. The rainfall of the last five days (R5) are presented in
312 Table 1. It can be observed that among all the events analyzed, there was no
313 rainfall at all during the previous five days for four events and for five events the
314 R5 was < 36 mm, corresponding to a dry condition. Five other events were
315 classified as having field capacity humidity, and two rain events considered as
316 saturated soil. The SSC during this period (2011-2015) was not high, except for
317 the events that occurred on 18/09/12 and 12/07/15 (Table 1). According to
318 studies conducted in this catchment between 2002 and 2016, the minimum and
319 maximum SCC recorded values are 0 and 13.7 g L^{-1}, respectively (Minella et
320 al., 2018). However, considering the duration and the surface runoff (Q_{runoff}) of a
321 certain event, the sediment yield (SY) may still be high. An example is the event
322 of 20/07/2011 that presented low average SSC (SSC_{ave} - 0.2 g L^{-1}) and a

maximum value of 0.6 g L^{-1}, but due to high Q_{runoff}, generated high SY (24.8 ton). The opposite situation was observed for the event that occurred on 12/07/2015, where the SSC_{ave} was higher, but the SY was lower, because the Q_{runoff} was much lower. Annual and event-based hydrographs and sedimentographs during sampling can be found in the supplementary material.

Figure 2 shows the preferential form of transport of each chemical element. A significant proportion of Ca^{2+}, K^{+}, Na^{+}, and Mg^{2+} transport occurred in dissolved form (47, 41, 39 and 28% respectively). In contrast, Mn, Fe, P, Cu, Si and Zn were mostly transported in particulate form (99, 97, 91, 90, 85 and 79%, respectively).

Table 1: Hydro-sedimentary variables monitored during 16 rainfall events from 2011 to 2015 in the Arvorezinha catchment.

3.2 Chemical element exports

Table 2 shows the number of rainfall events, the number of samples (n), minimum, average, and maximum concentrations for each element. A large number of samples were collected during the rising, peak and falling limbs of the hydrograph resulting in a total of 164 samples, although for some elements, mainly anions, only the samples of a restricted number of events (n= 7) could be analyzed (Table 2). The analyzed samples cover a wide range of concentrations, due to the variability of rainfall events in terms of magnitude and seasonality.

347 Table 2: Chemicals, total rainfall events, total of samples, maximum, mean and
348 minimum concentration, log (C) – log (Q) regression slopes (±SE) and CV_c/CV_Q
349 of dissolved and particulate elements during events from 2011 to 2015 in the
350 Arvorezinha catchment.
351
352 3.2.1 Dilution patterns
353 Analyzing separately the metric indices β and CV_C/CV_Q, the following
354 results were obtained with β < 0 significantly different from zero (p < 0.05): -
355 0.32 ± 0.11 for DOC and -0.12 ± 0.03 for Na^+; where their concentration
356 decreased when Q increased (Table 2). Although the β value for Cl^- was not
357 significantly different from zero (p < 0.06), its value was also < 0. The CV_C/CV_Q
358 values obtained for DOC and Cl^-, were 0.83 and 0.58, respectively, which are >
359 0.5, indicating a chemodynamic pattern (Table 2). In contrast, for Na^+, the value
360 of CV_C/CV_Q was 0.42, indicating a chemostatic pattern.
361
362 3.2.2 Enrichment patterns
363 For SSC and for the concentrations in particulate form of all the chemical
364 elements analyzed, the β values were > 0 (p < 0.05), with the exception of that
365 obtained for Zn, which was not statistically different from zero (p < 0.13). This
366 behavior indicates an enrichment (Table 2), and it was also observed for PO_4^{3-}
367 and Zn^{2+}. Similarly, the CV_C/CV_Q ratio was > 0.5 for all elements in particulate
368 form, SSC, PO_4^{3-} and Zn^{2+}, characterizing a chemodynamic pattern. In addition,
369 for some particulate elements (Ca, K, Mg, Mn and Zn) and for PO_4^{3-}, the
370 CV_C/CV_Q ratio is ≥ 1, which is classified as a strong chemodynamic pattern.
371

372 3.2.3 Chemostatic patterns

373 The concentration of NO_3^-, SO_4^{2-}, Ca^{2+}, K^+, Mg^{2+}, Cu^{2+}, Fe^{2+}, Mn^{2+} and
374 Si^{4+} showed little variations with water discharge, because β ~ 0. All these
375 elements, except for SO_4^{2-} (β = -0.09 ± 0.03, p < 0.01) and Ca^{2+} (β = -0.04 ±
376 0.02, p < 0.03), showed no significant difference from zero, at p < 0.05. The
377 chemostatic pattern was confirmed by CV_C/CV_Q ratio values ≤ 0.5 for NO_3^-,
378 SO_4^{2-}, Ca^{2+}, K^+ and Mg^{2+} (Table 2). However, Cu^{2+}, Fe^{2+}, Mn^{2+} and Si^{4+} were
379 associated with a CV_C/CV_Q ratio > 0.5, which would indicate a chemodynamic
380 pattern (Table 2).

381 When the two metric indices are combined, it is possible to obtain better
382 insights into the transport patterns of the analyzed elements (Gwenzi et al.,
383 2017) (Figure 3). A major part of the elements was characterized by an increase
384 in their concentration with increasing water discharge (β > 0; CV_C/CV_Q ≥ 0.5).
385 Furthermore, those elements such as dissolved PO_4^{3-} and Zn^{2+} were among
386 those with the strongest chemodynamic behavior (CV_C/CV_Q ≥ 1). In contrast,
387 those elements with β ~ 0 and CV_C/CV_Q < 0.5 showed a weak relationship
388 between their concentration and the water discharge, mainly Mg^{2+}, K^+, Ca^{2+},
389 NO_3^- and SO_4^{2-} (Figure 3). Na^+, Cl^- and DOC exhibit a dilution behavior.

390

391 3.3 Hysteresis and flushing analysis

392 The occurrence of a clockwise pattern was more frequent (> 50%) for K^+,
393 Fe^{2+}, Mn^{2+} and Na^+, SSC and for all particulate elements (Table 3). PO_4^{3-} and
394 particulate Na presented equal proportions of clockwise (50%) and
395 counterclockwise (50%) hysteresis behaviors. All particulate elements and SSC,
396 except for Zn, presented positive HI values. Fe^{2+}, Mn^{2+} and particulate Zn,

showed negative HI values (-1.18, -0.67 and -1.31, respectively), but the clockwise hysteresis pattern predominated. Among the dissolved chemical elements, only NO_3^-, K^+, Na^+, PO_4^{3-} and Si^{4+} showed positive HI values, although NO_3^- did not show a well-defined hysteresis pattern (Table 3).

For Cl^-, SO_4^{2-}, Ca^{2+}, Cu^{2+}, Mg^{2+}, Si^{4+}, Zn^{2+} and DOC, a dominance of counterclockwise patterns occurred (> 50%) which is supported by their negative HI values (Table 3). The only exception was observed for DOC and Si^{4+} that showed a positive HI value, with the occurrence of a few events with high HI values, resulting in a positive average value.

Similarly, all particulate elements and SSC presented positive FI values, indicating that their concentration increased during the hydrograph's rising limb (Table 3). All the dissolved elements, except for PO_4^{3-}, together with DOC showed negative values for FI (Table 3), indicating that their concentration decreased during the hydrograph's rising limb.

Table 3: Chemicals, mean Hysteresis Index (HI) and Flushing Index (FI) values and percentages of distinct hysteresis patterns during these events monitored from 2011 to 2015 in the Arvorezinha catchment.

When plotting FI *vs* HI, additional information may be derived to improve our understanding of the transport and the sources of these elements during the investigated rainfall events (Figure 4).

In Figure 4a, the elements with negative FI and positive HI are found (NO_3^-, Si^{4+}, K^+, Na^+ and DOC). These elements show a dilution effect and they are supplied by nearby sources, which is particularly well defined for DOC. The

422 dilution effect indicates that this element reaches the river from one of the main
423 flow pathways, which is hypothesized to be surface runoff, since organic carbon
424 concentrations are higher in the topsoil layers. However, the slight
425 predominance of the counterclockwise direction for DOC may be surprising
426 (56%, Table 3), as we expected a clockwise predominance when examining the
427 hysteresis behavior alone without considering other indices (Figure 4a). All
428 other elements are characterized by HI values close to zero, suggesting the
429 absence of well-defined hysteresis patterns (clockwise, counterclockwise, or
430 complex).

431 All the elements in particulate form, except Zn, SSC and dissolved PO_4^{3-}
432 are characterized by an increase in their concentrations during the rising limb
433 (Figure 4b). Furthermore, the source of these elements is expected to be in the
434 vicinity of the catchment outlet, being delivered during the rising limb and
435 depleted during the falling limb (Figure 4b). Particulate Zn is an exception
436 because its main behavior is counterclockwise according to the HI value (its
437 source is expected to be far from the catchment outlet) (Figure 4d). This
438 analysis suggests that at the beginning of an event there is an increase of these
439 element during the rising limb and it is supplied by more distant sources.
440 However, for most events (57%, Table 3), the particulate Zn shows a clockwise
441 pattern. For most events, the HI value was positive and close to zero for Zn. For
442 only two events the HI values were more negative (-4.69 and -5.65 for the
443 events occurred in 01/10/2011 and 20/09/2013, respectively), which makes the
444 result for this element inconclusive.

445 Cl^-, SO_4^{2-}, Ca^{2+}, Mg^{2+}, Cu^{2+} and Mn^{2+} showed a dilution effect and they
446 are likely supplied by distant sources, well characterized for Ca^{2+}, Cu^{2+}, Mn^{2+},

447 Fe^{2+} and Zn^{2+} that present more negative values (-0.22, -0.36, -0.67 and -1.18,
448 respectively) (Figure 4c). The other three elements (Cl^-, SO_4^{2-}, Mg^{2+}) were
449 characterized by HI values close to zero (-0.03, -0.05 and -0.06, respectively),
450 suggesting that they are supplied by closer sources during the event, than the
451 other four elements found in Figure 4c.
452
453 **4. DISCUSSION**
454 The rainfall events investigated in the current research covered a
455 pluriannual period, including different seasons and climatic phenomena. The
456 year 2015 was classified as El Niño (NOAA) for Southern Brazil with annual
457 rainfall exceeding 2,498 mm in the study site (Barros, 2016). In the agricultural
458 crop season of 2011/2012, a La Niña phenomenon was registered, which may
459 cause periods of drought in Southern Brazil (NOAA). Therefore, different
460 hydrological behavior occurs in the catchment and they were covered by the
461 period of sampling.
462 The chemical elements that can be strongly adsorbed by clays and iron
463 oxides, were mainly transported in particulate form, including P, Fe and Mn
464 with 91, 97 and 99%, respectively. In contrast, large proportions of ions such as
465 Ca, K and Na were transported in dissolved form (48, 41 and 39%,
466 respectively). However, it should be noted that these values refer to the average
467 value calculated for the entire set of 16 rainfall events (Figure 2). When
468 analyzing the dissolved and particulate proportions for each individual rainfall
469 event, these proportions can be different. Accordingly, during those rainfall
470 events with high SSC, almost 100% of the elements with a high affinity with
471 sediment particles, such as P, Mn, and Fe, were transported in particulate form.

For events with lower sediment concentrations, the proportion of these elements in dissolved form increased. In contrast, elements with a low affinity for sediment particles, such as Ca and K, were mainly transferred in dissolved form whatever the SSC conditions observed during the event.

Three different transport regimes are described for the analyzed elements in the next sections, namely: (i) chemodynamic - enrichment, (ii) chemodynamic – dilution and (iii) chemostatic.

4.1 Drivers for enrichment patterns

All the elements in particulate form (Ca, Cu, Fe, K, Mg, Mn, Na, P, Si and Zn), as well as SSC and dissolved PO_4^{3-} showed a concentration enrichment with increased discharges. Botter et al. (2019) observed a similar behavior for total phosphorous (Particulate P + PO_4^{3-}), which shows higher concentrations with increasing discharges.

Sediment availability for transport is dependent on the kinetic energy of rainfall during previous events and on the occurrence of new sediment pulses, that may be triggered by landslides or channel bank erosion (Wymore et al., 2019). As the Arvorezinha catchment did not experience any landslide during the study period, the main sediment supply to the stream is associated with the occurrence of interill and rill erosion in cultivated areas (57% of the total sediment) (Tiecher et al., 2015). However, other potential sources were outlined as delivering a significant proportion of sediment and particle-bound elements. Unpaved roads were shown to provide 23% of the sediment (Tiecher et al., 2015) with preferential connections with the river network (Barros, 2016). This high connectivity between the roads and the stream systems allows the quick

497 delivery of readily available sediment to the stream (Figure 1). These results are
498 consistent with the findings of the current research showing that the sources of
499 particle-bound elements are close from the monitoring station (as these
500 parameters showed a clockwise pattern in > 50% of the events), which may
501 explain the rapid mobilization of the sediment and the elements bound to or
502 contained in the particles (Table 3, Figure 4).

503 PO_4^{3-} was the only compound in dissolved form that presented the same
504 behavior as the particulate elements (Figure 4). Bender et al. (2018) evaluating
505 the P (dissolved and particulate form) dynamics in the same place of the
506 present study and through eight rain events already verified a strong
507 correspondence between the PO_4^{3-} behavior with its particulate form. This is
508 likely related to the saturation of soils with the use of high doses of phosphate
509 fertilizers for tobacco cultivation. Pellegrini et al. (2010) showed that sediment
510 eroded from soils cultivated with tobacco were saturated with phosphates and
511 their desorption capacity was extremely high and fast. The dissolved form of
512 nutrients essential to the development of agricultural crops, such as PO_4^{3-}, is
513 the form that they will be available in the aqueous medium and can trigger new
514 reactions or processes (Tang et al., 2019). In this catchment, a high availability
515 of PO_4^{3-} is found in water and sediments, as already observed in a previous
516 study (Bender et al., 2018). A study conducted in France and compiling 40-year
517 records of water quality data from 293 monitoring stations showed that the
518 mitigation of phosphorus pollution reduced the concentrations in this substance
519 and altered the corresponding C – Q slopes (Moatar et al., 2017). Therefore,
520 understanding how the transfer of these elements occurs is of fundamental
521 importance, and is linked to the climatic conditions associated with the

522 characteristics of the catchment responsible for generating runoff and erosive
523 processes.
524
525 4.2 Drivers for dilution patterns
526 Fe^{2+}, Zn^{2+}, Cu^{2+} and Mn^{2+} exhibited an increase in their concentration in
527 the rising limb, but during the event, other flow pathways with low concentration
528 in these elements have reached the catchment outlet and contributed to a
529 dilution phenomenon (Figure 3). All these elements displayed counterclockwise
530 patterns, reflecting their supply by sources that are located far from the
531 catchment outlet (Figure 4c).
532 More specifically, Fe^{2+}, Si^{4+} and Mn^{2+} are released by natural weathering
533 processes and they remain in soluble form in the soil water compartment.
534 Previous studies that examined the hydrological dynamics in the Arvorezinha
535 catchment revealed that subsurface and base flows may supply 60 to 80% of
536 the streamflow during a rainfall event in autumn and winter (Barros, 2016;
537 Robinet et al., 2018). Accordingly, the greater frequency of counterclockwise
538 hysteresis behavior patterns may be explained by an important contribution of
539 subsurface flow during rainfall events.
540 Dissolved Cu^{2+} and Zn^{2+} showed a similar behavior than Fe^{2+}, Si^{4+} and
541 Mn^{2+} (Figures 3 and 4). The increased concentrations measured at the
542 beginning of the rainfall event were likely due to the release of these elements
543 by weathering processes, as young soils (Acrisols, Cambisols and Leptsols) of
544 basaltic origin are found in this catchment. In addition, in this area, low inputs of
545 Cu^{2+} and Zn^{2+} are expected from the use of fertilizers and agrochemicals

546 (exogenous solutes), which reinforces the different behavior observed
547 compared to that of DOC and dissolved Na^+ and Cl^-.

548 Na^+, Cl^- and DOC are preferentially transported with surface runoff, due
549 to their high concentrations in the topsoil layer. The high concentration of Na^+
550 and Cl^- in water may be explained using inorganic fertilizers for tobacco
551 cultivation ($NaNO_3$ and KCl), which occupied 15 to 20% of the total catchment
552 surface area between 2011 to 2015. Finally, organic carbon is concentrated in
553 the topsoil layer due to inputs from cover crops; although the levels found may
554 vary depending on land use and soil management (Boix-Fayos et al., 2017;
555 Endale et al., 2017).

556

557 4.3 Chemostatic patterns

558 In general, Mg^{2+}, K^+, Ca^{2+}, NO_3^- and SO_4^{-2} showed a very weak C - Q
559 relationship. Several sources (anthropogenic and geogenic) may supply these
560 elements, which can come from the storage of these solutes in the soil and by
561 surface runoff. Thus, elements such as K^+, may not have their concentration
562 altered with the increase of Q, because all flow pathways to the river may have
563 similar concentrations, causing no dilution effect nor enrichment with the
564 changes in the water discharge. In White Clay Creek, Pennsylvania – USA, the
565 K^+ was the only element among those analyzed that presented a chemostatic
566 behavior and a complex hysteresis pattern, as it can be considered a biological
567 solute, geological weathering and additional K^+ inputs from exogenous sources
568 such as fertilizer (Rose et al., 2018). In Arvorezinha catchment, the production
569 of the tobacco requires high inputs of lime and industrial fertilizers
570 (anthropogenic source) containing K^+, NO_3^- and SO_4^{-2}. Both ions have a low

bridging energy to clay, oxides, and organic matter, which may facilitate their release into the soil and possibly be transported by subsurface flow towards the catchment outlet. In addition, another fraction of these elements can be carried by surface runoff, due to their higher concentration on the topsoil layer. Na^{+}, NH_4^{+}, K^{+}, Mg^{2+}, Ca^{2+} were already shown to be associated with geogenic sources in a study conducted under a subtropical climate in Brazil (Piazza et al., 2018). In Nevada, USA, eight small river catchments were monitored (0.5 to 2.3 km^2) and during the 8-years study period, Mg^{2+}, K^{+}, Ca^{2+}, Cl^{-}, Na^{+} and SO_4^{-2} revealed a chemostatic behavior under temperate climate, although an opposite situation was observed for NH_4^{+} and NO_3^{-} (Hunsaker and Johnson, 2017).

5. CONCLUSIONS

The results show the strong correspondence between the magnitude of the rainfall event and the preferred form of transportation of the chemical elements. The water discharge is linked to the magnitude of the rainfall event and the generation of surface runoff, the main responsible for the transport of sediment and potential contaminants to the river. This can be attributed to the strong erosive potential of rainfall in subtropical region combined to use and soil management, that have an impact on the hydrological dynamics of the catchment. Practices that may reduce the supply of water (by surface runoff) and sediment to the river network will also minimize the transport of elements in particulate form (Ca, Cu, Fe, K, Mg, Mn, Na, P, Si and Zn), which is the preferred form of chemical elements transport in this catchment. In the same

595 way, PO_4^{3-} concentration increased with the surface runoff, having the same
596 behavior of particulate elements, preferentially transferred by surface runoff.
597 Most of the dissolved chemical elements are associated to both element
598 sources (geogenic/anthropogenic) and flow pathways (base, subsurface and
599 surface flow). Thus, elements that are not preferably transported by surface
600 runoff, such as geogenic (Fe^{2+}, Zn^{2+}, Cu^{2+}, Mn^{2+} and Si^{4+}), reduce their
601 concentration with the increase in water discharge, and the dilution process
602 occurs. DOC, Na^{+} and Cl^{-} also have a dilution regime export (concentrations
603 decrease with the increase of Q). However, their source is anthropogenic
604 through fertilization and soil organic matter and mainly transported by the
605 surface runoff.
606 The chemostatic regime export is linked to chemical elements that are
607 supplied by more than one flow pathway (Mg^{2+}, K^{+}, Ca^{2+}, NO_3^{-} and SO_4^{2-}), due
608 its potential contribution by both geogenic and anthropogenic source.
609 Overall, the results show that despite a small data set, it was possible to
610 understand the transport of some important chemical elements (nutrients,
611 geochemicals and metals) in a subtropical environment and it could be better
612 understood when the different metric indices were used together. These
613 insights are fundamental to design strategies to control surface runoff and
614 erosive process, because as we have observed, they seem to be the main
615 responsible for the chemical elements transport in this region.
616

617 **6. ACKNOWLEDGEMENTS**

618

The authors would like to thank to Conselho Nacional de Pesquisa - CNPq, Coordenação de Aperfeiçoamento de Pessoal de Nível Superior - CAPES, Financiadora de Estudos e Projetos - FINEP, government of Rio Grande do Sul state and Sindicato Interestadual da Indústria do Tabaco - SindiTabaco for providing financial support. Furthermore, the authors are grateful to the “Mais Água” project and FAPERGS PRONEX n° 008/2009 projects for their support.

7. REFERENCES

Alvares, C.A., Stape, J.L., Sentelhas, P.C., De Moraes Gonçalves, J.L., Sparovek, G., 2013. Köppen’s climate classification map for Brazil. Meteorol. Zeitschrift 22, 711–728. https://doi.org/10.1127/0941-2948/2013/0507

Barros, C.A.P. de, 2016. Dinâmica Dos Escoamentos Na Modelagem Da Produção De Sedimentos Em Uma Pequena Bacia Rural. PhD thesis. Federal University of Santa Maria.

Basu, N.B., Destouni, G., Jawitz, J.W., Thompson, S.E., Loukinova, N. V., Darracq, A., Zanardo, S., Yaeger, M., Sivapalan, M., Rinaldo, A., Rao, P.S.C., 2010. Nutrient loads exported from managed catchments reveal emergent biogeochemical stationarity. Geophys. Res. Lett. 37, 1–5. https://doi.org/10.1029/2010GL045168

Bender, M.A., dos Santos, D.R., Tiecher, T., Minella, J.P.G., de Barros, C.A.P., Ramon, R., 2018. Phosphorus dynamics during storm events in a subtropical rural catchment in southern Brazil. Agric. Ecosyst. Environ. 261, 93–102. https://doi.org/10.1016/j.agee.2018.04.004

644 Boix-Fayos, C., Martínez-Mena, M., Cutillas, P.P., de Vente, J., Barberá, G.G.,
645 Mosch, W., Navarro Cano, J.A., Gaspar, L., Navas, A., 2017. Carbon
646 redistribution by erosion processes in an intensively disturbed catchment.
647 Catena 149, 799–809. https://doi.org/10.1016/j.catena.2016.08.003

648 Botter, M., Burlando, P., Fatichi, S., 2019. Anthropogenic and catchment
649 characteristic signatures in the water quality of Swiss rivers: A quantitative
650 assessment. Hydrol. Earth Syst. Sci. 23, 1885–1904.
651 https://doi.org/10.5194/hess-23-1885-2019

652 Cargnin, A.P., De Aveline Bertê, A.M., De Oliveira Lemos, B., De Oliveira, S.B.,
653 2013. Atlas socioeconômico do Rio Grande do Sul: quinze anos
654 acompanhando as transformações do estado. Geo UERJ 2.
655 https://doi.org/10.12957/geouerj.2013.8200

656 Chow, V. Te, Maidment, D.R., Mays, L.W., 1988. Aplied Hydrology, McGraw-
657 Hil. ed.

658 CONAB, 2019. Acompanhamento da Safra Brasileira. Cia. Nac. Abast. 5, 1–
659 113.

660 Deuschle, D., Minella, J.P.G., Hörbe, T. de A.N., Londero, A.L., Schneider,
661 F.J.A., 2019. Erosion and hydrological response in no-tillage subjected to
662 crop rotation intensification in southern Brazil. Geoderma 340, 157–163.
663 https://doi.org/10.1016/j.geoderma.2019.01.010

664 Didoné, E.J., Minella, J.P.G., Merten, G.H., 2015. Quantifying soil erosion and
665 sediment yield in a catchment in southern Brazil and implications for land
666 conservation. J. Soils Sediments 15, 2334–2346.
667 https://doi.org/10.1007/s11368-015-1160-0

668 Duvert, C., Gratiot, N., Evrard, O., Navratil, O., Némery, J., Prat, C., Esteves,
669 M., 2010. Drivers of erosion and suspended sediment transport in three
670 headwater catchments of the Mexican Central Highlands. Geomorphology
671 123, 243–256. https://doi.org/10.1016/j.geomorph.2010.07.016

672 Endale, D.M., Potter, T.L., Strickland, T.C., Bosch, D.D., 2017. Sediment-bound
673 total organic carbon and total organic nitrogen losses from conventional
674 and strip tillage cropping systems. Soil Tillage Res. 171, 25–34.
675 https://doi.org/10.1016/j.still.2017.04.004

676 Godsey, S.E., Kirchner, J.W., Clow, D.W., 2009. Concentration-discharge
677 relationships reflect chemostatic characteristics of US catchments. Hydrol.
678 Process. 23, 1844–1864. https://doi.org/10.1002/hyp.7315

679 Gwenzi, W., Chinyama, S.R., Togarepi, S., 2017. Concentration-discharge
680 patterns in a small urban headwater stream in a seasonally dry water-
681 limited tropical environment. J. Hydrol. 550, 12–25.
682 https://doi.org/10.1016/j.jhydrol.2017.04.029

683 Helsel, D.R., Hirsch, R.M., 2002. Statistical Methods in Water Resources,
684 Studies in Environmental Sciences. United States Geological Survey.
685 https://doi.org/10.13140/RG.2.2.36048.10248

686 Hunsaker, C.T., Johnson, D.W., 2017. Concentration-discharge relationships in
687 headwater streams of the Sierra Nevada, California. Water Resour. Res.
688 53, 7869–7884. https://doi.org/10.1002/2016WR019693

689 Knapp, J.L., Freyberg, J. von, Studer, B., Kiewiet, L., Kirchner, J., 2020.
690 Concentration-discharge relationships vary among hydrological events,
691 reflecting differences in event characteristics. Hydrol. Earth Syst. Sci.

692 Discuss. 1–27. https://doi.org/10.5194/hess-2019-684

693 Lawler, D.M., Petts, G.E., Foster, I.D.L., Harper, S., 2006. Turbidity dynamics
694 during spring storm events in an urban headwater river system: The Upper
695 Tame, West Midlands, UK. Sci. Total Environ. 360, 109–126.
696 https://doi.org/10.1016/j.scitotenv.2005.08.032

697 Lloyd, C.E.M., Freer, J.E., Johnes, P.J., Collins, A.L., 2016. Technical Note:
698 Testing an improved index for analysing storm discharge-concentration
699 hysteresis. Hydrol. Earth Syst. Sci. 20, 625–632.
700 https://doi.org/10.5194/hess-20-625-2016

701 Londero, A.L., Minella, J.P.G.G., Deuschle, D., Schneider, F.J.A.A., Boeni, M.,
702 Merten, G.H., 2018. Impact of broad-based terraces on water and sediment
703 losses in no-till (paired zero-order) catchments in southern Brazil. J. Soils
704 Sediments 18, 1159–1175. https://doi.org/10.1007/s11368-017-1894-y

705 Merten, G.H., Araújo, A.G., Biscaia, R.C.M., Barbosa, G.M.C., Conte, O., 2015.
706 No-till surface runoff and soil losses in southern Brazil. Soil Tillage Res.
707 152, 85–93. https://doi.org/10.1016/j.still.2015.03.014

708 Merten, G.H., Horowitz, A.J., Minella, J.P.G., Moro, M., 2014. Determinação da
709 concentração de sedimentos em suspensão em rios com o uso de
710 turbidímetro. Porto Alegre, Brasil.

711 Minella, J.P.G., Merten, G.H., Barros, C.A.P., Ramon, R., Schlesner, A., Clarke,
712 R.T., Moro, M., Dalbianco, L., 2018. Long-term sediment yield from a small
713 catchment in southern Brazil affected by land use and soil management
714 changes. Hydrol. Process. 32, 200–211. https://doi.org/10.1002/hyp.11404

715 Moatar, F., Abbott, B.W., Minaudo, C., Curie, F., Pinay, G., 2017. Elemental
716 properties, hydrology, and biology interact to shape concentration-
717 discharge curves for carbon, nutrients, sediment, and major ions. Water
718 Resour. Res. 53, 1270–1287. https://doi.org/10.1002/2016WR019635

719 Musolff, A., Schmidt, C., Selle, B., Fleckenstein, J.H., 2015. Catchment controls
720 on solute export. Adv. Water Resour. 86, 133–146.
721 https://doi.org/10.1016/j.advwatres.2015.09.026

722 Pellegrini, J.B.R., Dos Santos, D.R., Gonçalves, C.S., Copetti, A.C.C.,
723 Bortoluzzi, E.C., Tessier, D., 2010. Impacts of anthropic pressures on soil
724 phosphorus availability, concentration, and phosphorus forms in sediments
725 in a Southern Brazilian watershed. J. Soils Sediments 10, 451–460.
726 https://doi.org/10.1007/s11368-009-0125-6

727 Piazza, G.A., Dupas, R., Gascuel-Odoux, C., Grimaldi, C., Pinheiro, A.,
728 Kaufmann, V., 2018. Influence of hydroclimatic variations on solute
729 concentration dynamics in nested subtropical catchments with
730 heterogeneous landscapes. Sci. Total Environ. 635, 1091–1101.
731 https://doi.org/10.1016/j.scitotenv.2018.03.394

732 Ramon, R., 2017. Kinetic energy measurement of rainfall and defining a pluvial
733 index to estimate erosivity in Arvorezinha/RS. Master thesis. Federal
734 University of Santa Maria.

735 Ramon, R., Minella, J.P.G., Merten, G.H., de Barros, C.A.P., Canale, T., 2017.
736 Kinetic energy estimation by rainfall intensity and its usefulness in
737 predicting hydrosedimentological variables in a small rural catchment in
738 southern Brazil. Catena. https://doi.org/10.1016/j.catena.2016.07.015

739 Robinet, J., Minella, J.P.G., de Barros, C.A.P., Schlesner, A., Lücke, A.,
740 Ameijeiras-Mariño, Y., Opfergelt, S., Vanderborght, J., Govers, G., 2018.
741 Impacts of forest conversion and agriculture practices on water pathways in
742 Southern Brazil. Hydrol. Process. 32, 2304–2317.
743 https://doi.org/10.1002/hyp.13155

744 Rose, L.A., Karwan, D.L., Godsey, S.E., 2018. Concentration-discharge
745 relationships describe solute and sediment mobilization, reaction, and
746 transport at event and longer timescales. Hydrol. Process. 32, 2829–2844.
747 https://doi.org/10.1002/hyp.13235

748 Rumsey, C.A., Miller, M.P., Schwarz, G.E., Hirsch, R.M., Susong, D.D., 2017.
749 The role of baseflow in dissolved solids delivery to streams in the Upper
750 Colorado River Basin. Hydrol. Process. 31, 4705–4718.
751 https://doi.org/10.1002/hyp.11390

752 Shreve, E.A., Downs, A.C., 2005. Quality-Assurance Plan for the Analysis of
753 Fluvial Sediment by the U.S. Geological Survey Kentucky Water Science
754 Center Sediment Laboratory. Geol. Surv. Open-File Rep. -1230. 35.

755 SILVEIRA, L., CHARBONNIER, F., GENTA, J.L., 2000. The antecedent soil
756 moisture condition of the curve number procedure. Hydrol. Sci. J. 45, 3–12.
757 https://doi.org/10.1080/02626660009492302

758 Tang, X., Li, R., Wu, M., Zhao, W., Zhao, L., Zhou, Y., Bowes, M.J., 2019.
759 Science of the Total Environment In fl uence of turbid fl ood water release
760 on sediment deposition and phosphorus distribution in the bed sediment of
761 the Three Gorges. Sci. Total Environ. 657, 36–45.
762 https://doi.org/10.1016/j.scitotenv.2018.12.011

763 Thomas, Z., Abbott, B.W., Troccaz, O., Baudry, J., Pinay, G., 2016. Proximate
764 and ultimate controls on carbon and nutrient dynamics of small agricultural
765 catchments. Biogeosciences 13, 1863–1875. https://doi.org/10.5194/bg-13-
766 1863-2016

767 Thompson, S.E., Basu, N.B., Lascurain, J., Aubeneau, A., Rao, P.S.C., 2011.
768 Relative dominance of hydrologic versus biogeochemical factors on solute
769 export across impact gradients. Water Resour. Res. 47, 1–20.
770 https://doi.org/10.1029/2010WR009605

771 Tiecher, T., Caner, L., Minella, J.P.G., Santos, D.R. dos, 2015. Combining
772 visible-based-color parameters and geochemical tracers to improve
773 sediment source discrimination and apportionment. Sci. Total Environ.
774 527–528, 135–149. https://doi.org/10.1016/j.scitotenv.2015.04.103

775 U.S. EPA, 1997. Method 300.1, Revision 1.0: Determination of Inorganic Anions
776 in Drinking Water by Ion Chromatography. Washington, DC.

777 U.S. EPA, 1996. EPA Method 3050B, Revision 2: Acid Digestion of Sediments,
778 Sludges, and Soils. Washington, DC.

779 U.S. EPA, 1994. Method 200.7, Revision 4.4: Determination of macro and trace
780 elements in rare earth magnesium cast iron by inductively coupled plasma
781 atomic emission spectrometry. Washington, DC.

782 Vaughan, M.C.H., Bowden, W.B., Shanley, J.B., Vermilyea, A., Schroth, A.W.,
783 2019. Shining light on the storm: in-stream optics reveal hysteresis of
784 dissolved organic matter character. Biogeochemistry 143, 275–291.
785 https://doi.org/10.1007/s10533-019-00561-w

786 Verheyen, D., Van Gaelen, N., Ronchi, B., Batelaan, O., Struyf, E., Govers, G.,
787 Merckx, R., Diels, J., 2015. Dissolved phosphorus transport from soil to
788 surface water in catchments with different land use. Ambio 44, 228–240.
789 https://doi.org/10.1007/s13280-014-0617-5

790 Von Freyberg, J., Studer, B., Kirchner, J.W., 2017. A lab in the field: High-
791 frequency analysis of water quality and stable isotopes in stream water and
792 precipitation. Hydrol. Earth Syst. Sci. 21, 1721–1739.
793 https://doi.org/10.5194/hess-21-1721-2017

794 Wan, Y., Wan, L., Li, Y., Doering, P., 2017. Decadal and seasonal trends of
795 nutrient concentration and export from highly managed coastal catchments.
796 Water Res. 115, 180–194. https://doi.org/10.1016/j.watres.2017.02.068

797 Williams, M.R., Livingston, S.J., Penn, C.J., Smith, D.R., King, K.W., Huang, C.
798 hua, 2018. Controls of event-based nutrient transport within nested
799 headwater agricultural watersheds of the western Lake Erie basin. J.
800 Hydrol. 559, 749–761. https://doi.org/10.1016/j.jhydrol.2018.02.079

801 Wymore, A.S., Leon, M.C., Shanley, J.B., McDowell, W.H., 2019. Hysteretic
802 response of solutes and turbidity at the event scale across forested tropical
803 montane watersheds. Front. Earth Sci. 7.
804 https://doi.org/10.3389/feart.2019.00126

805

806

807

808 Figure 1 – Location of the study site in Brazil and the hydro-sedimentary
809 monitoring within the catchment.

810

811 Figure 2 – Average distribution of chemical elements in dissolved and
812 particulate forms during the rainfall events monitored from 2011 to 2015.

813

814 Figure 3: Plot of log (C) – log (Q) regression slope – β *versus* CV_C/CV_Q for all
815 elements determined in the current study. The plotted values correspond to the
816 mean of those measurements conducted on all the samples analyzed during
817 the 2011 – 2015 period. Error bars represent ± 1 Standard Error β. SSC:
818 suspended sediment concentration; DOC: dissolved organic carbon.

819

820 Figure 4: Plots of median hysteresis index versus median flushing index for
821 chemical across all sampled rainfall events from 2011 to 2015. SSC: suspended
822 sediment concentration; DOC: dissolved organic carbon. HI and FI values are
823 normalized considering their maximum value equal to 1.

824

825

826

Table 1

Table 1: Hydro-sedimentary variables monitored during events from 2011 to 2015 in the Arvorezinha catchment.

Data	T	R	R5	Q_{total}	Q_{base}	Q_{runoff}	Q_{peak}	C	SSC_{peak}	SSC_{ave}	SY
	min	----------	----------	mm	----------	----------	$L\ s^{-1}$	%	$g\ L^{-1}$		ton
20/07/2011	1340	127	44	92.7	37.5	55.2	3399.4	43.4	0.6	0.2	24.8
01/10/2011	350	17	0	0.81	0.61	0.2	57.7	1.2	0.2	0.1	0.1
05/07/2012	1460	95	0	16.5	10.6	6.2	536.4	6.4	0.4	0.2	2.4
26/08/2012	2040	27	15	1.0	0.9	0.1	44.2	0.5	0.2	0.1	0.3
09/09/2012	540	26	0	9.1	8.9	0.2	35.6	0.7	0.3	0.1	0.1
18/09/2012	430	110	27	44.3	19.3	25	1470.8	22.7	5.3	1.1	20.6
12/03/2013	480	27	58	5.6	4.7	0.9	235.6	3.4	0.2	0.1	0.6
24/08/2013	*	64	16	0.9	**	**	45.5	**	0.1	0.1	0.1
20/09/2013	1980	84	18	47.6	22.2	25.4	785.3	30.2	2.2	0.7	70.6
26/10/2013	245	36	52	6.3	3.6	2.7	463.6	7.5	1.0	0.4	3.3
19/03/2014	430	34	35	2.1	1.3	0.9	125.9	2.5	0.7	0.3	0.9
23/07/2014	950	83	0	26.7	17.0	9.7	1034.5	11.7	1.1	0.2	6.4
06/09/2014	390	42	8	7.4	5.2	2.2	258.4	5.2	0.4	0.2	1.2
30/09/2014	950	42	51	20.2	12.5	7.7	520.5	18.2	0.2	0.1	1.9
08/07/2015	1370	48	36	19.7	17.8	1.9	536.4	4.0	0.3	0.1	2.2
12/07/2015	*	87	86	22.5	17.0	5.5	599.5	6.3	5.4	0.4	6.6

* Events that lasted more than one day. ** This event was long, and the rainfall was of low intensity; accordingly, during the period of sampling, the flow level did not rise. T = duration of the rainfall, R = rainfall depth, R5 = antecedent rainfall of the last five days, Q_{total}= total flow, Q_{base}= total base flow, Q_{runoff}= total surface runoff; Q_{peak}= peak flow, C = surface runoff coefficient, SSC_{peak}= peak suspended sediment concentration, SSC_{ave}= average suspended sediment concentration, SY= sediment yield.

Table 2

Table 2: Chemicals, total rainfall events, total of samples, maximum, mean and minimum concentration, log (C) – log (Q) regression slopes (±SE) and CV_C/CV_Q of dissolved and particulate elements during events from 2011 to 2015 in the Arvorezinha catchment.

Chemical	Events	Data	Maximum	Mean	Minimum	β	CV_C/CV_Q
SSC	16	164	4.4	0.3	0.0	0.52 (± 0.08)†	1.16
DOC	15	114	10.4	1.8	0.0	-0.32 (± 0.11)†	0.83
Dissolved							
Cl^-	7	53	16.4	3.0	0.6	-0.10 (± 0.05)	0.58
NO_3^-	7	53	2.7	1.2	0.4	-0.06 (± 0.03)	0.23
SO_4^{2-}	7	53	5.3	2.7	0.6	-0.09 (± 0.03)†	0.24
Ca^{2+}	16	164	4333.7	2183.8	660.9	-0.04 (± 0.02)†	0.16
Cu^{2+}	16	142	31.6	2.1	0.0	0.05 (± 0.06)	1.05
Fe^{2+}	16	163	2034.6	303.7	0.0	0.07 (± 0.12)	0.89
K^+	16	164	4548.3	2611.6	534.0	-0.01 (± 0.02)	0.13
Mg^{2+}	16	164	1273.3	743.0	297.5	-0.02 (± 0.01)	0.11
Mn^{2+}	16	126	22.0	3.6	0.0	0.08 (± 0.09)	0.74
Na^+	16	143	4492.4	1210.7	0.0	-0.12 (± 0.03)†	0.42
PO_4^{3-}	16	150	642.5	27.7	0.0	0.23 (± 0.08)†	1.41
Si^{4+}	16	163	10223.6	1621.7	0.0	0.01 (± 0.08)	0.63
Zn^{2+}	16	164	77.7	10.6	0.3	0.14 (± 0.06)†	0.70
Particulate							
Ca	12	105	72709	2191.3	0.0	0.62 (± 0.11)†	2.05
Cu	11	95	98.6	12.3	0.0	0.35 (± 0.14)†	0.96
Fe	12	118	111452.0	13408.7	290.3	0.66 (± 0.07)†	0.97
K	12	103	28784.1	3218.0	0.0	0.46 (± 0.09)†	1.02
Mg	12	110	18021.1	1710.1	0.0	0.51 (± 0.08)†	1.10
Mn	12	118	4631.5	472.5	9.0	0.77 (± 0.08)†	1.03
Na	11	89	9438.0	1376.1	0.0	0.45 (± 0.15)†	0.99
P	12	114	1936.1	203.8	0.0	0.60 (± 0.07)†	0.90
Si	12	112	53759.4	9383.1	0.0	0.65 (± 0.08)†	0.91
Zn	11	81	489.4	25.3	0.0	0.20 (± 0.13)	1.48

SSC: suspended sediment concentration - g L^{-1}; DOC: dissolved organic carbon (mg L^{-1}); Cl^-, NO_3^-, SO_4^{2-} are expressed in mg L^{-1}, whereas the other elements are expressed in µg L^{-1}, SE: standard error. † Significant different from zero at $p < 0.05$.

Table 3

Table 3: Chemicals, mean Hysteresis Index (HI) and Flushing Index (FI) values and percentages of distinct hysteresis patterns during these events monitored from 2011 to 2015 in the Arvorezinha catchment.

Chemical	HI	FI	% Clockwise	% Counterclockwise	%Complex
SSC	1.48	0.75	85	15	0
DOC	2.63	-0.09	44	56	0
Dissolved					
Cl^-	-0.03	-0.20	43	57	0
NO_3^-	0.03	-0.34	43	43	14
SO_4^{2-}	-0.05	-0.38	43	57	0
Ca^{2+}	-0.22	-0.38	38	62	0
Cu^{2+}	-0.36	-0.08	36	64	0
Fe^{2+}	-1.18	-0.15	54	46	0
K^+	0.05	-0.04	54	38	8
Mg^{2+}	-0.06	-0.30	38	68	0
Mn^{2+}	-0.67	-0.04	67	33	0
Na^+	0.01	-0.71	55	45	0
PO_4^{3-}	0.69	0.28	50	50	0
Si^{4+}	0.05	-0.67	46	54	0
Zn^{2+}	-1.43	-0.10	23	77	0
Particulate					
Mg	1.16	0.59	80	20	0
Ca	0.56	0.38	80	20	0
Cu	1.02	0.44	89	11	0
Mn	1.80	0.66	90	10	0
Fe	1.18	0.67	80	20	0
Na	0.24	0.30	50	50	0
K	0.42	0.51	70	30	0
P	0.86	0.63	80	10	10
Si	1.36	0.59	100	0	0
Zn	-1.31	0.59	57	43	0

SSC: suspended sediment concentration; DOC: dissolved organic carbon

Figure 1

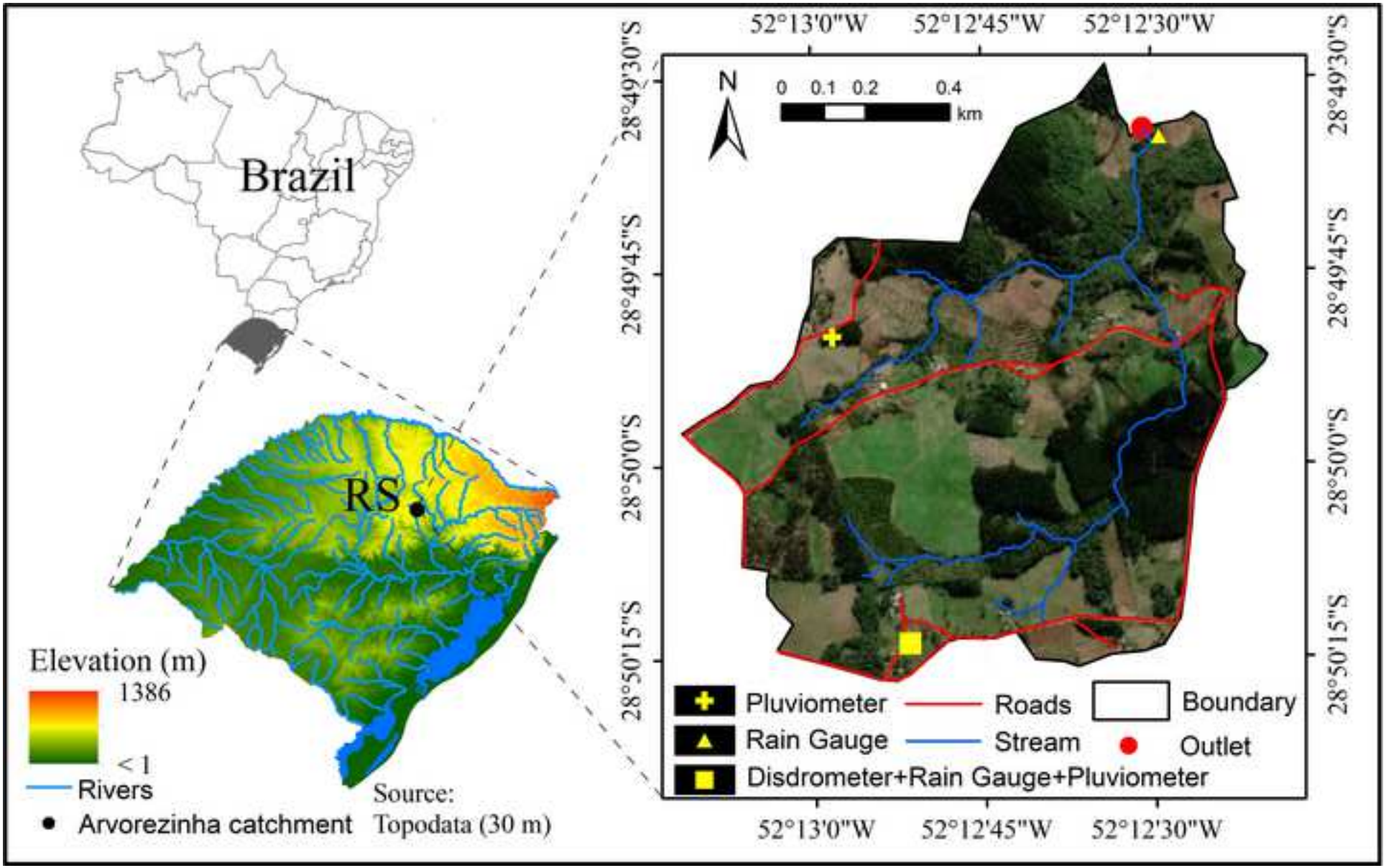
Brazil
RS
Elevation (m)
1386
< 1
Rivers
Arvorezinha catchment
Source:
Topodata (30 m)
52°13'0"W
52°12'45"W
52°12'30"W
28°49'30"S
28°49'45"S
28°50'0"S
28°50'15"S
N
0 0.1 0.2 0.4
km
Pluviometer
Rain Gauge
Disdrometer+Rain Gauge+Pluviometer
Roads
Stream
Boundary
Outlet

Figure 2

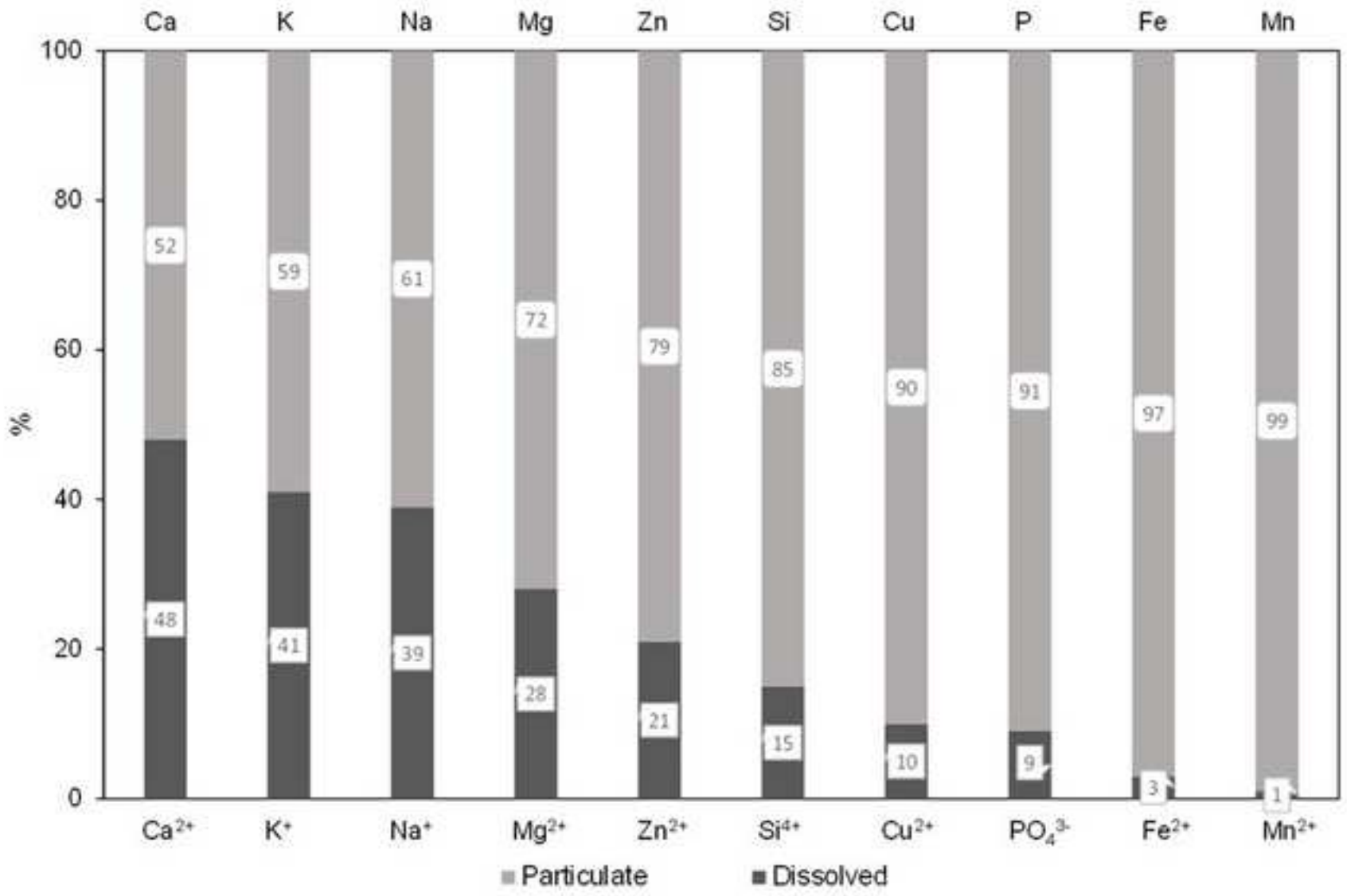
Ca
K
Na
Mg
Zn
Si
Cu
P
Fe
Mn
100
80
60
40
20
0
%
52
59
61
72
79
85
90
91
97
99
48
41
39
28
21
15
10
9
3
1
Ca2+
K+
Na+
Mg2+
Zn2+
Si4+
Cu2+
PO43-
Fe2+
Mn2+
Particulate
Dissolved

Figure 3

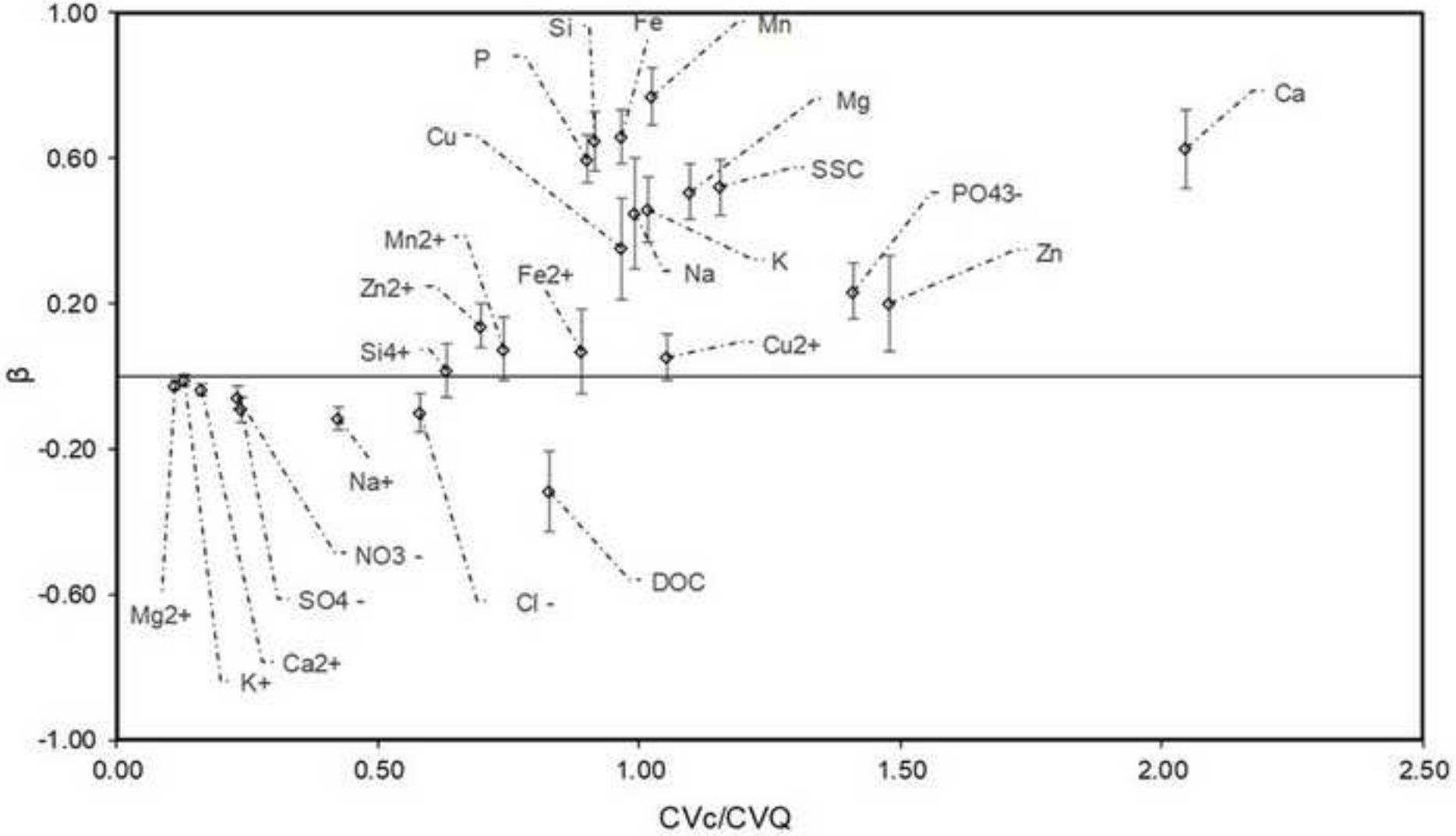
1.00
0.60
0.20
-0.20
-0.60
-1.00
β
0.00
0.50
1.00
1.50
2.00
2.50
CVc/CVQ
Si
Fe
Mn
P
Mg
Ca
Cu
SSC
PO43-
Mn2+
K
Zn
Na
Zn2+
Fe2+
Si4+
Cu2+
Na+
NO3 -
DOC
SO4 -
Cl -
Mg2+
Ca2+
K+

Figure 4

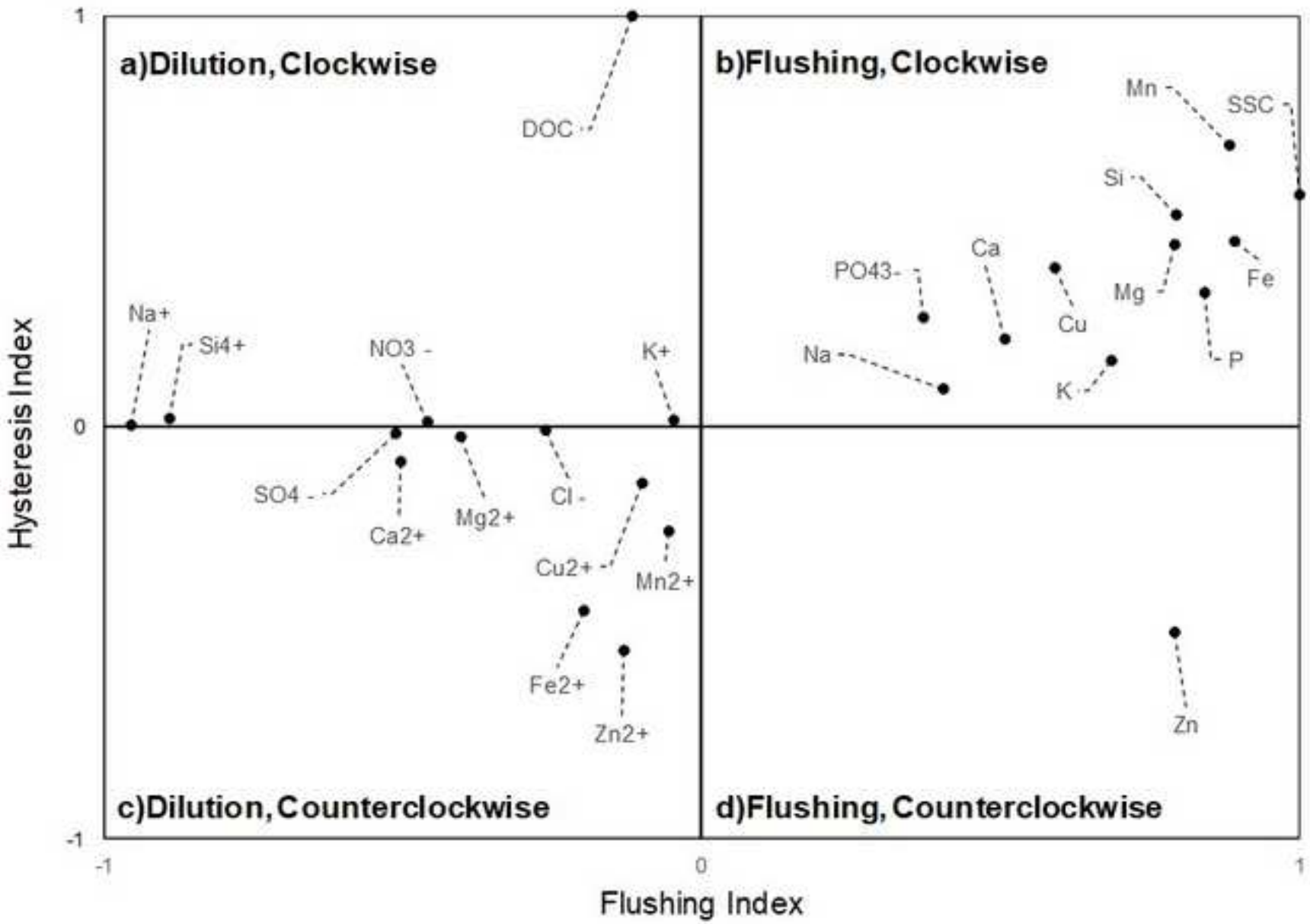
a)Dilution, Clockwise
b)Flushing, Clockwise
c)Dilution, Counterclockwise
d)Flushing, Counterclockwise
DOC
Na+
Si4+
NO3 -
K+
SO4 -
Ca2+
Mg2+
Cl -
Cu2+
Mn2+
Fe2+
Zn2+
Mn
SSC
Si
Ca
PO43-
Mg
Fe
Cu
Na
K
P
Zn
1
0
-1
-1
0
1
Hysteresis Index
Flushing Index

*Graphical Abstract